High-Precision 3-D Measurements on Moving Objects

Matthias Laimer, Daniel Wertjanz, Peter Gsellmann, Georg Schitter, *Senior Member, IEEE*, and Ernst Csencsics, *Member, IEEE*

***Abstract*—This article presents a six degree of freedom dual stage sample-tracking system for compensating relative motion and enabling high precision 3-D surface measurements on moving objects. The system comprises a 3-D measurement module for fine positioning, which is mounted as end effector to an industrial robot being used for coarse positioning. The embedded free-floating measurement platform actively tracks a sample to locally establish lab-like conditions for the integrated 3-D measurement tool. A dual stage position control scheme is designed to dynamically reposition the long-range actuator for tracking a moving sample, such that the measurement platform is kept within its actuation range. Experiments on a moving sample demonstrate a residual tracking error of 490 nm rms in sample-motion direction, corresponding to a performance increase by factor 32, as compared to the state-of-the-art approach. The analysis of the performed measurements shows an uncertainty reduction by one order of magnitude to 610 nm rms, enabling 3-D measurements on a moving sample with submicrometer precision.**

***Index Terms*—3-D imaging, inline measurement systems, mechatronics.**

I. Introduction

FOR today's high-tech manufacturing industry, flexibility is a key aspect to meet global trends, such as resource-efficient production, as well as to rapidly respond to fluctuating market demands [1], [2]. This is accompanied by a steady increase in product quality, while further raising the production efficiency [3]. In this relation, robotic inline measurement systems are considered as key enablers to keep up with these global trends [4]. As a consequence of the increased demand for automation in the quality assessment steps during manufacturing [5], the integration of industrial robots (IRs) for inspection tasks has grown significantly in recent decades [6], [7].

Compared to conventional high-precision measurement tools (MTs), such as coordinate measuring machines, which may require multiple un-/loading steps for a single workpiece and are typically operating offline, robotic measurement systems offer higher versatility due to their kinematic structure and the flexible integration into a production line, increasing the overall production efficiency [8], [9]. To not impair the throughput, inspection processes have to be conducted within the existing production cycle time [10], [11]. Particularly in production systems, such as the automotive sector, robotic measurement systems operating along assembly lines on moving objects are widely deployed [6], [10]. With repeatabilities down to tens of microns, IRs have successfully replaced single-purpose tools in many industries [7], [12].

However, the integration of robotic measurement systems into industrial applications with single or even submicrometer precision, such as required for the inspection of optics or stacked IC devices, is still an unsolved challenge [13], [14]. Part of this limitation is the finite stiffness of IRs, resulting from the serial link of multiple rigid bodies, making it hardly feasible to position or move the robot end effector with micrometer precision [7]. Similar to the limited positioning precision of IRs, environmental vibrations induced by industrial processes cause relative motion between the robotic end effector and the sample, which impairs the overall positioning performance [15].

To compensate for disturbing relative motion between an inline measurement system and a sample, an active sample-tracking approach can be employed [16]. Recently, a high-precision 3-D measurement system has been proposed, which comprises a levitated measurement platform (MP) [17]. By means of feedback control, a contactless stiff link between sample and MT is established, compensating relative motion in six degree of freedoms (DOFs). So far, the system uses a long-range coarse actuator to manually position the MT relative to a static sample with arbitrary spatial orientation [17]. For the combined actuation of both positioning systems, dual stage actuation and control is a viable approach. Its applications range from precise machining [18], [19] to the positioning of high-precision wafer stages in the semiconductor industry [20]. To enable measurements on moving samples, it combines the long-range and flexible positioning capability of the coarse

Manuscript received 13 December 2023; revised 21 May 2024 and 28 June 2024; accepted 9 July 2024. Recommended by Technical Editor S. Ibaraki and Senior Editor D. Chen. This work was supported in part by the Austrian Federal Ministry of Labour and Economy, in part by the National Foundation for Research, Technology and Development, in part by the Christian Doppler Research Association, in part by the Micro-Epsilon Atensor GmbH and MICRO-EPSILON-MESSTECHNIK GmbH & Co.K.G., and in part by the Hochschuljubilaeumsfonds of the city of Vienna, Austria, under Grant H-260744/2020. *(Matthias Laimer and Daniel Wertjanz contributed equally to this work.) (Corresponding author: Matthias Laimer.)*

The authors are with the Christian Doppler Laboratory for Precision Measurements in Motion, Automation and Control Institute (ACIN), TU Wien, 1040 Vienna, Austria (e-mail: laimer@acin.tuwien.ac.at).

Color versions of one or more figures in this article are available at https://doi.org/10.1109/TMECH.2024.3435999.

Digital Object Identifier 10.1109/TMECH.2024.3435999

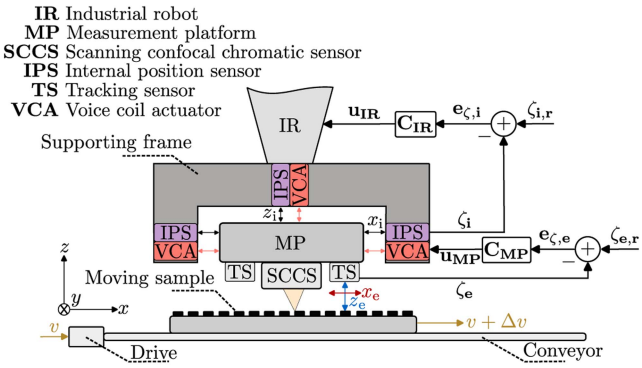

Fig. 1. Dual stage-controlled positioning system for precision measurements on moving samples. A constant relative position x_e and z_e between the MP and sample is maintained by the feedback controller C_{MP}. The feedback controller C_{IR} repositions the IR based on the internal MP positions x_i and z_i.

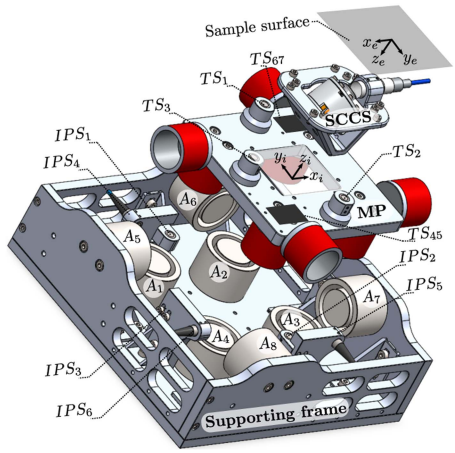

Fig. 2. Exploded view of the functional components of the 3-D measurement module. A1 ... A8 are the VCAs to actuate the MP in all 6 DOFs. IPS1 ... IPS6 and TS1 ... TS67 are the internal position and TSs, respectively. The SCCS is embedded into the MP as 3-D measurement tool (MT).

actuation system with the short-stroke positioning range of the high-precision actuator.

The contribution of this article is the integrated design of a dual stage positioning system with six DOFs enabling the precise tracking of moving samples with submicrometer precision, such that high-resolution 3-D measurements can be performed in motion. The concept and integrated design of the sample-tracking 3-D measurement system is introduced in Section II, followed by a description of the experimental setup in Section III. Based on the identified IR dynamics, a tailored motion control scheme enabling the long-range tracking of moving samples is designed in Section IV. The tracking performance and the achieved 3-D measurement precision in motion are evaluated in Section V. Finally, Section VI concludes this article.

II. Inline 3-D Measurements on Moving Objects

A. System Concept

The concept of the 3-D measurement system for inline applications is shown in Fig. 1. With the sample being placed on a conveyor system, the total sample velocity $v_S = v + \Delta v$ is a superposition of the process-induced conveyor velocity v and a disturbance-induced motion Δv. The sample-tracking 3-D measurement module [21] is mounted as end effector to an IR. To compensate the disturbing relative motion between the scanning confocal chromatic sensor (SCCS) as 3-D MT and the moving sample, a dual stage concept is developed in a parent–child control architecture [22] in Section IV. The SCCS is embedded into an electromagnetically levitated MP, which is capable of tracking the sample with submicrometer precision [23]. In this relation, the MP is the precision and the IR the coarse positioning system. Tracking sensors (TSs) are integrated in the MP to measure the external position $\boldsymbol{\zeta}_\mathbf{e}$ relative to the sample, i.e., x_e and z_e in Fig. 1. A constant relative position $\boldsymbol{\zeta}_{\mathbf{e,r}}$, is maintained based on the measured deviation $\mathbf{e}_{\zeta,\mathbf{r}}$ by means of feedback control ($\mathbf{C_{MP}}$, with $\mathbf{u_{MP}}$ being the control output), establishing the desired stiff link between SCCS and sample.

Additional internal position sensors (IPSs) are integrated, which measure the MP's internal position $\boldsymbol{\zeta}_\mathbf{i}$ relative to the IR. Based on the measured deviation $\mathbf{e}_{\zeta,\mathbf{i}}$ from its center position $\boldsymbol{\zeta}_{\mathbf{i,r}}$, the IR is repositioned based on the control output $\mathbf{u_{IR}}$ of the feedback controller $\mathbf{C_{IR}}$, such that the MP is kept within its limited actuation range. In this way, precise sample-tracking on the long-range is achieved, enabling the desired high-precision 3-D measurements on moving objects.

B. Measurement Module

Eight voice coil actuators (VCAR0087-0062-00 A, SuptMotion, Suzhou, China), each capable of supplying 20 N continuous force as illustrated in Fig. 2, are integrated to enable quasi-zero stiffness actuation of the MP in six DOFs, which mechanically decouple it from disturbances induced by the limited positioning precision of the IR [17]. Voice coil actuators (VCAs) A_1–A_4 are used to actuate the MP in its out-of-plane DOFs ($z_i, \phi_{x_i}, \phi_{y_i}$), while the VCAs A_5–A_8 enable the actuation in the in-plane DOFs (x_i, y_i, ϕ_{z_i}) [23]. With the MP being actuated within the air gaps (500 μm between stator and mover) of the VCAs, an actuation range of about $\pm 175 \mu$m and ± 3mrad in the translational and rotational DOFs is achieved. Six capacitive IPSsm (IPS_1–IPS_6 CSH05, Micro-Epsilon, Ortenburg, Germany) providing a measurement range of 500 μm with 17 nm rms position noise at a measurement rate of 40 kHz, are used to measure the MP's position relative to the IR, which serves as feedback for the IR repositioning control ($\mathbf{C_{IR}}$ in Fig. 1), being synthesized and discussed in detail in Section IV-B.

Three capacitive out-of-plane TS (TS_1–TS_3, CSH05, Micro-Epsilon, Ortenburg, Germany) and two in-plane TSs based on photosensitive detectors (TS_{45} and TS_{67}, S5991-01, Hamamatsu Photonics K.K., Hamamatsu, Japan) are integrated to measure the relative position between the MP and the sample in six DOFs [23]. To enable contactless high-precision 3-D measurements, the embedded compact SCCS as described in [21] is

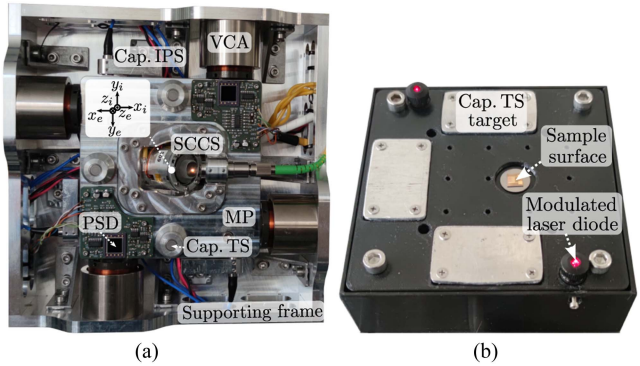

Fig. 3. Setup enabling high precision sample-tracking. (a) Detailed view of the sample-tracking measurement module with the SCCS as 3-D MT being embedded into the MP. (b) Sample box equipped with targets and markers for the out-of-plane and in-plane TSs [17].

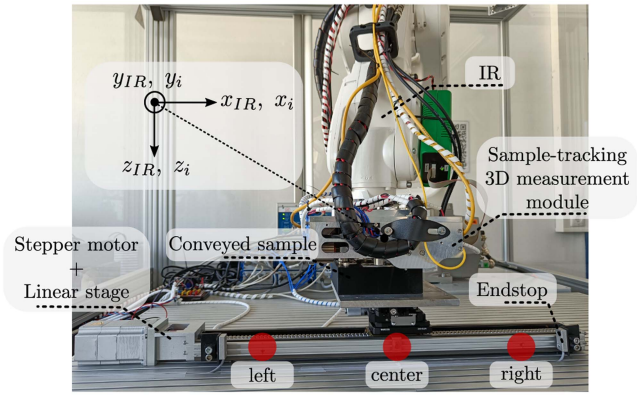

Fig. 4. Experimental setup of the dual stage positioning system for high-precision 3-D measurements on moving samples. The long-range motion of the sample being conveyed by the linear stage is actively tracked using a dual stage control structure.

used. It deploys a high precision 1-D confocal chromatic sensor (CCS) (IFS2404-2, Micro-Epsilon, Ortenburg, Germany) in combination with a 2-D fast steering mirror [24] to manipulate the optical path, enabling measurements in three dimensions. The spot diameter of the CCS is 10μm. The SCCS achieves a lateral and axial resolution down to 2.5μm and 77 nm within a measurement volume of 0.35 mm $\times$ 0.25 mm $\times$ 1.8 mm, respectively, and frame rates of up to 1 fps. A more detailed description can be found in [21].

The positioning uncertainty of the feedback-controlled MP is about 25 nm rms in the translational out-of-plane (z) and about 200 nm rms in the translational in-plane DOFs (x and y). With integrated aluminum targets for the capacitive sensors and modulated laser diodes (LDM650/1LJM, Roithner Lasertechnik GmbH, Vienna, Austria) as markers for the position sensitive detector, the sample box shown in Fig. 3(b) is used as the carrier of the sample surface to be inspected [23].

III. Experimental System Setup

The sample-tracking 3-D measurement module [see Fig. 3(a)] is mounted as end effector to the IR (KUKA KR 10 R900-2, KUKA AG, Augsburg, Germany) with a working radius of 0.9 m. Fig. 4 shows the experimental system setup. To emulate an industrial production line, a motorized 400 mm linear stage is used, with the two-phase stepper motor being actuated by a motor driver (TMC2209-V1.2, BIGTREETECH, Ltd., Shenzhen, China). By applying a frequency-modulated rectangular signal to the drive of the stepper motor, the conveyor velocity can be varied. The linear stage's velocity is mechanically limited to a maximum of 15 mm s^{-1}. As can be seen in Fig. 4, the IR's tool center point (TCP) and MP's internal coordinate system are selected to coincide in a common origin.

A rapid prototyping system (MicroLabBox, dSpace GmbH, Paderborn, Germany) is used for controlling the entire sample-tracking 3-D measurement module. To enable the desired dual stage control of the robotic positioning system, a second, industrial DAQ system (components of Beckhoff Automation GmbH & Co. KG, Verl, Germany) is used, acquiring the internal MP position (see Fig. 1). The robot sensor interface (RSI) (KUKA

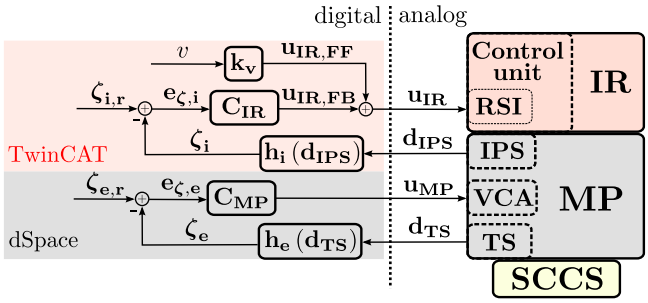

Fig. 5. Simplified block diagram of the dual stage-controlled robotic 3-D measurement system. The SCCS is used as MT and integrated in the MP. The feedback controller $\mathbf{C_{MP}}$ is used to maintain a constant position between SCCS and the sample. Based on the measured internal MP position, the IR is repositioned by means of the feedback controller $\mathbf{C_{IR}}$ to maintain the MP within its limited actuation range.

AG, Augsburg, Germany) is used as real-time communication interface between the industrial DAQ system and the control unit of the IR, operating at a sampling frequency of 250 Hz (4 ms sampling time). It enables the repositioning of the IR's TCP based on external sensor signals and allows the design and implementation of external control loops one level above the internal KUKA control. The IR reposition control is implemented on an engineering computer deploying TwinCAT 3 (Beckhoff Automation GmbH & Company KG, Verl, Germany) and executed on an isolated physical processor core of the engineering PC with a sampling frequency of 12.5 kHz.

IV. System Analysis and Control Design

The measurement module in Fig. 3(a) comprises a 6-DOF single input single output (SISO) PID sample-control architecture, enabling the precise positioning of the MP relative to a sample [23]. A simplified block diagram of the dual stage positioning system is illustrated in Fig. 5. Based on the measured tracking error $\mathbf{e_{\zeta,e}}$, the output $\mathbf{u_{MP}}$ of the sample-tracking controller $\mathbf{C_{MP}}$ is applied to the VCA-based actuation system.

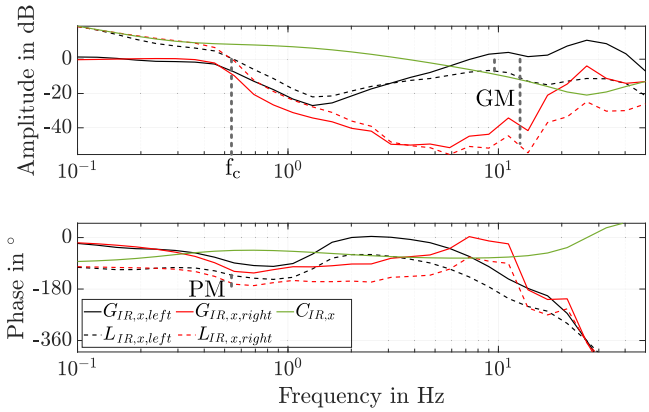

Fig. 6. Identification of the IR dynamics in motion direction (DOF x) in the left and right IR position on the conveyor system ($G_{\text{IR},x,\text{left}}$ and $G_{\text{IR},x,\text{right}}$). A pair of antiresonance and resonance is identified in a frequency range of 1 to 30 Hz. A single controller $C_{\text{IR},x}$ is designed for the entire conveyor travel range.

Embedded in the MP, the compact and lightweight SCCS is capable of performing high-precision 3-D measurements [21].

To enable the tracking of moving samples on the long-range, the IR needs to be robustly and precisely repositioned in six DOFs based on the internal position data, such that the MP is maintained within its limited actuation range. Therefore, the IR dynamics are identified and a tailored IR repositioning control $\mathbf{C_{IR}}$ (see Fig. 5) is designed in the following sections.

A. Identification of IR Dynamics

With the integrated sample-tracking controller $\mathbf{C_{MP}}$ [23], the IR dynamics along the conveyor travel range are identified in a first step. Considering the IR as a rigid-body system, its dynamics vary for different poses [25], which is why the dynamics are identified in three positions (left, center, and right) indicated in red in Fig. 4. Therefore, a sinusoidal sweep $A\sin(2\pi fk)$ is consecutively applied to the reference position $\boldsymbol{\zeta}_{\mathbf{i,r}}$ in each DOF of the position-controlled IR in the range of 0.1 to 50 Hz, with the amplitude A being set to 10μm and 0.1mrad for the translational and rotational DOFs, respectively. Throughout the identification process in a certain pose, the MP's sample-tracking control is enabled, i.e., a stiff link to the conveyor system is established.

The dynamics for each DOF of the IR are obtained by

$$G_{\text{IR},j} = \frac{\zeta_{i,j}}{\zeta_{i,j,r}}, \quad j \in \{x,\, y,\, z,\, \phi_x,\, \phi_y,\, \phi_z\} \tag{1}$$

with $\zeta_{i,j}$ being the MP's internal position in DOF j and $\zeta_{i,j,r}$ the IR reference position. The identified IR dynamics are exemplarily shown for the motion direction x in Fig. 6 (solid black and red lines) at the left and right IR position on the conveyor system. As can be seen, a pair of antiresonance and resonance is identified within the frequency range of 1 to 30 Hz in both poses, caused by the mechanical decoupling of the harmonic drive gears in the joints [26], [27]. The crosstalk between the individual DOFs of the IR for frequencies up to 0.5 Hz is 10 dB lower than the respective system dynamics (data not shown), which is why a SISO control architecture is pursued in the following controller synthesis.

B. Dual Stage Control Design

Based on the identified IR dynamics, a SISO PI control architecture is designed one level above the internal KUKA control. The discretized PI control for the kth time step in standard form [28]

$$u_{\text{IR}}(k) = k_p\left(e_{\zeta,i}(k) + \frac{T_s}{T_i}\sum_{l=0}^{k} e_{\zeta,i}(l)\right) \tag{2}$$

is synthesized for each DOF, with k_p being the proportional gain, T_i integrator time constant, and T_s the corresponding sampling time. Since the RSI cycle time is 4 ms (cycle frequency is 250 Hz) but the internal MP's internal position signals are acquired with a sampling time of 80μs, the IR repositioning error $e_{\zeta,i}$ is oversampled by a factor of 50, allowing moving averaging of $e_{\zeta,i}$ to smooth higher frequency components.

As can exemplarily be seen in the identified dynamics $G_{x,\text{left}}$ and $G_{x,\text{right}}$ in Fig. 6, similar magnitudes and phases below the antiresonance for the left and right IR position on the conveyor system are obtained, enabling the use of the same PI parameters for the IR repositioning along the entire conveyor range. The six individual controllers are synthesized in a loop-shaping approach based on the measured dynamics in the IR's center position (see Fig. 4). To suppress the excitation of the identified resonances without significantly impairing the phase margin (PM), notch filters

$$H_{N,j}(s) = \frac{s^2 + 2\delta\pi\nu + 4\pi^2\nu^2}{s^2 + 2\delta\rho\pi\nu + 4\pi^2\nu^2}, \quad j \in \{x,\, y,\, z,\, \phi_x,\, \phi_y,\, \phi_z\} \tag{3}$$

with δ defining the width and ρ the depth at a certain frequency ν, are designed for each DOF j. The resulting IR repositioning controller yields

$$C_{\text{IR},j} = C_{\text{PI},j}H_{N,j}, \quad j \in \{x,\, y,\, z,\, \phi_x,\, \phi_y,\, \phi_z\} \tag{4}$$

with $C_{\text{PI},j}$ being the transfer function of the designed controller in (2) for a respective DoF j. Considering the conveyed sample motion direction (see Fig. 4), the highest IR control effort is required in DOF x. Therefore, a controller design tradeoff is made, maximizing the cross-over frequency under the aspect of still providing a robust IR controller over the entire conveyor travel range. A cross-over frequency f_c of 550 mHz yields a robust gain and PM of 14 dB and 45°, respectively, for the IR being in the center position. As shown in Fig. 6, the PM decreases to 20°, while traveling toward the right position on the conveyor system. In the left position, the PM increases up to 50°.

For the remaining DOFs, lower IR repositioning control effort is expected. To keep the crosstalk between the axes at a minimum, sufficient PM and gain margin (GM) of at least 50° and 10 dB for the translational DOFs and 100° and 10 dB for the rotational DOFs are targeted in the controller synthesis.

The measured loop gain of the IR repositioning $L_{\text{IR},j}$ and the sample-tracking controller $L_{\text{MP},j}$, $\quad j \in \{x,\, y,\, z,\, \phi_x,\, \phi_y,\, \phi_z\}$ in the translational and rotational DOFs are presented in Fig. 7.

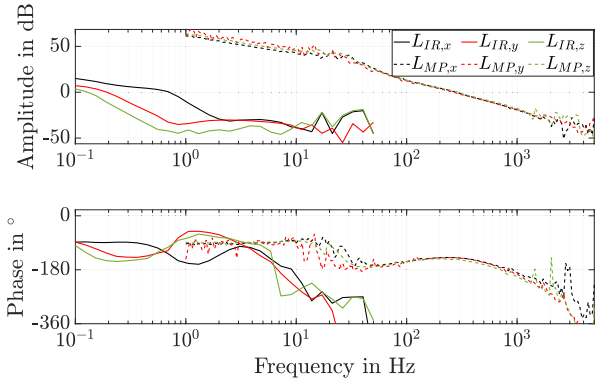

(a)

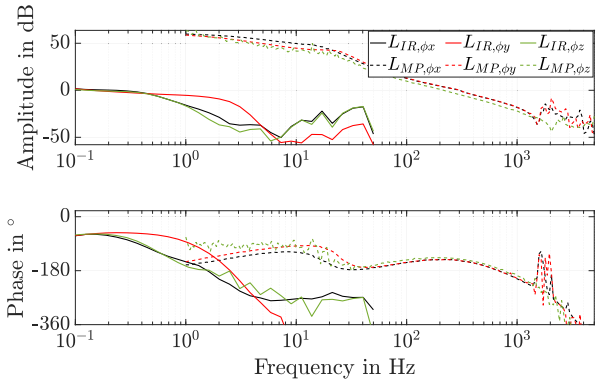

(b)

Fig. 7. Measured loop gain of the designed 6-DOF dual stage control. (a) Loop gain of the translational and (b) Rotational DOFs. The cross-over frequencies of the IR repositioning and the sample-tracking controllers are spectrally separated by about three decades.

TABLE I
MEASURED CROSS-OVER FREQUENCIES, GAIN, AND PMS

(a) Translational DOFs.

DOF	IR repositioning			Sample-tracking		
	f_c	GM	PM	f_c	GM	PM
x	0.55 Hz	14 dB	45°	289 Hz	16 dB	41°
y	0.18 Hz	11 dB	60°	284 Hz	15 dB	40°
z	0.11 Hz	12 dB	55°	301 Hz	12 dB	35°

(b) Rotational DOFs.

DOF	IR repositioning			Sample-tracking		
	f_c	GM	PM	f_c	GM	PM
ϕ_x	0.34 Hz	23 dB	113°	302 Hz	12 dB	36°
ϕ_y	0.14 Hz	12 dB	124°	303 Hz	12 dB	33°
ϕ_z	0.14 Hz	23 dB	128°	225 Hz	18 dB	43°

(a) For the Translational and (b) for the rotational DOFs of the IR repositioning (center position) and the sample-tracking controller.

As can be seen, each loop gain of the 6-DOF sample-tracking control is designed with a cross-over frequency of about 300 Hz. The measured crossover frequencies as well as the PMs and GMs are summarized in Table I. A -3 dB IR repositioning and sample-tracking bandwidth (BW) of about 1 and 450 Hz is achieved, respectively.

To further increase the performance of the IR repositioning control, the a priori knowledge of the conveyor velocity is considered by an additional feedforward controller (see Fig. 5). The constant $\mathbf{k_v}$ converts the conveyor reference velocity v into an IR position signal for each cycle. The resulting control output $\mathbf{u_{IR}}$ is a superposition of the feedback $\mathbf{u_{FB}}(\mathbf{k})$ and the feedforward controller output $\mathbf{u_{FF}}(\mathbf{k})$.

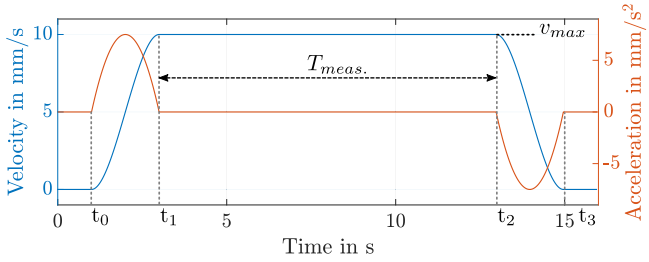

Fig. 8. Sample motion trajectory. Within the time interval $[t_0, t_1]$, the sample is accelerated from zero to a targeted velocity v_{max}. The sample velocity is kept constant for 10 s during the interval $T_{\text{meas.}} = [t_1, t_2]$ before it gets decelerated back to zero during the interval $[t_2, t_3]$.

V. EXPERIMENTAL PERFORMANCE EVALUATION

For the performance evaluation of the dual stage-controlled system, the measurement module is aligned to the sample box (see Fig. 4), i.e., all TSs are in range. To enable a performance comparison with state-of-the-art robotic measurement systems, a benchmark scenario is defined. In a state-of-the-art robotic measurement system without MP, the MT is directly mounted to an IR. This is equivalent to mechanically fixing the MP with the robot arm and disabling the sample-tracking control. The integrated TS can then be used as a measure for the relative motion. Due to the measurement range of the out-of-plane sensors of 500μm, operation with entirely disabled tracking control is, however, not possible. For this reason, a relaxed benchmark scenario is used. The sample-tracking control BW is reduced to 1 Hz, which keeps the sensors in range but essentially disables the disturbance rejection. The lateral sample motion tracking is disabled but robot-related oscillations are still suppressed due to the quasi-zero stiffness actuated MP. The relaxed benchmark scenario with 1 Hz tracking BW, thus, already represents an improvement as compared to the actual state-of-the-art case.

A. Dual Stage-Controlled Tracking of a Moving Target

With consideration of the linear stage's maximum velocity of 15 mm s^{-1} (see Section III) and adding a sufficient safety margin, samples are conveyed with velocities of up to 10 mm s^{-1} to be robustly tracked. The third-order velocity trajectory shown in Fig. 8 is applied to the conveyor system, ensuring a smooth acceleration and deceleration phase. Within the time intervals $[t_0, t_1]$ and $[t_2, t_3]$, the sample is accelerated from standstill up to $v = 10$ mm s^{-1} and decelerated back to zero, respectively. In the interval $[t_1, t_2]$, the velocity v is kept constant for 10s, serving as time slot for 3-D measurements with the SCCS (see Section V-B). Since the MP actively tracks the sample motion, the rms value of the internal MP position error can be used to quantify the performance of the dual stage-controlled robotic system. A value close to zero indicates that the MP is kept close

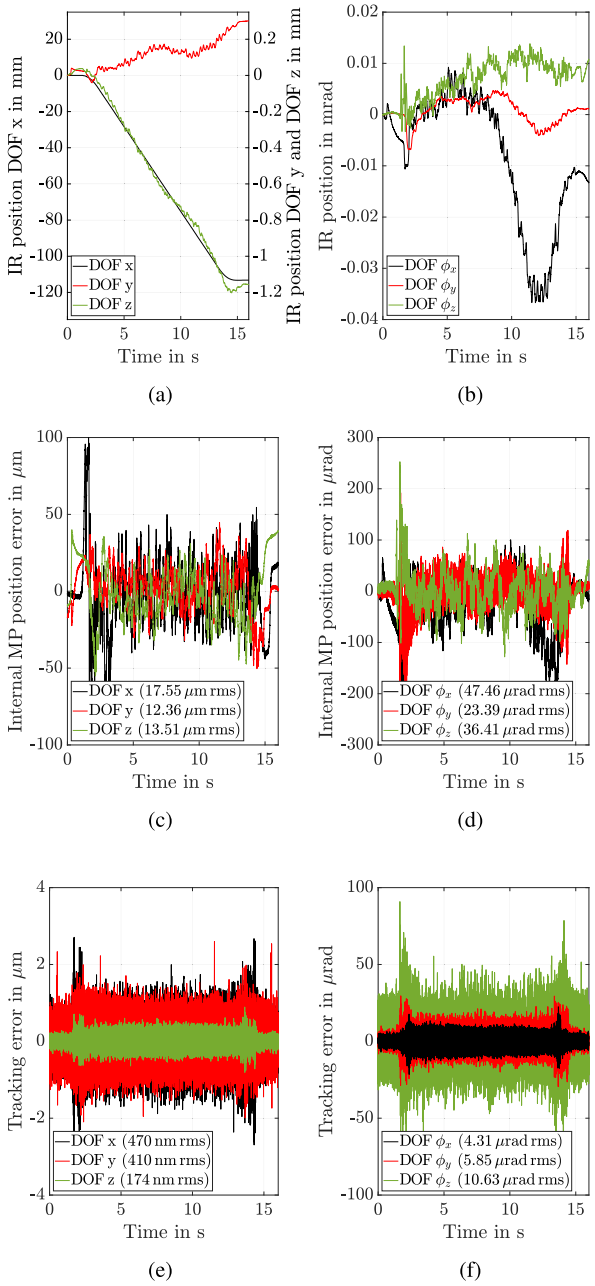

Fig. 9. Evaluated sample-tracking performance in 6-DOFs for the performed target motion trajectory of Fig. 8. (a) and (b) Measured IR motion. (c) and (d) Internal MP position error and (e) and (f) Sample-tracking error in six DOFs.

to its center position, leaving a larger extent of the actuation range for tracking higher frequency disturbance-induced target motions. The IR repositioning and tracking performance of the dual stage-controlled robotic system is evaluated within the time interval $T_{\text{meas.}} = [t_1, t_2] = 10\text{s}$, i.e., $v = \text{const.}$

In Fig. 9, the IR's TCP motion, as well as the MP's internal position and tracking error in six DOFs are shown for the applied velocity trajectory (see Fig. 8). As can be seen in Fig. 9(a) and (b), an IR motion in all six DOFs is required to maintain the MP within its actuation range.

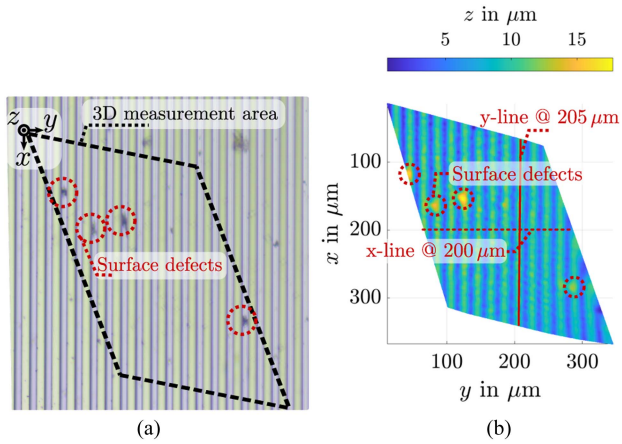

Fig. 10. Reference measurement of a test surface under laboratory conditions. (a) Microscope image of the grating structure with a pitch of 20μm. (b) 3-D measurement under static, lab conditions (no disturbances and motion).

In sample motion direction (DOF x), the IR is repositioned along a travelling range of more than 100 mm, indicated in black in Fig. 9(a). Considering the MP's actuation range (see Section II-B), the system's tracking range is increased by about three orders of magnitude. In the translational DOFs, the internal MP position error is kept below 20μm rms [see Fig. 9(c)], leaving the MP almost 90 % of the actuation range to track higher frequency sample motion. For a constant velocity $v = 10$ mm s^{-1}, residual sample-tracking errors below 500 nm rms and 200 nm rms are achieved in the translational in- and out-of-plane DOFs [see Fig. 9(e)]. The deviation in the tracking performance can be explained by the different sensing principles and the related noise floors of the in- and out-of-plane TSs (see Section II-B) [29]. Similar behavior can be recognized in the tracking error of the rotational DOFs [see Fig. 9(f)].

B. High-Precision 3-D Measurements in Motion

To prove the feasibility of precision measurements on moving objects, the 3-D measurement performance is evaluated, for 1) the defined benchmark scenario in Section V and 2) the proposed dual-stage controlled positioning system. A silicon grating structure (Nanuler Calibration Standard, Applied NanoStructures Inc., Mountain view, CA, USA) with a pitch of 20 μm is used and placed on the sample box [see Fig. 3(b)]. A microscope image of the sample under test is shown in Fig. 10(a), with several surface defects located within the 3-D measurement range. The measurement under static lab conditions is presented in Fig. 10(b), with the grating pitch as well as the surface defects clearly visible. To achieve such conditions, the MP actively tracks the sample surface to compensate for disturbing relative motion between SCCS and the sample caused by environmental vibrations, while the IR is at standstill and mechanically braked. The SCCS conducts the 3-D measurement point-by-point by scanning the sample surface with a Lissajous trajectory, achieving a framerate of 0.1 fps. The parallelogram-shaped measurement range is caused due to the alignment of the CCS [21]. As

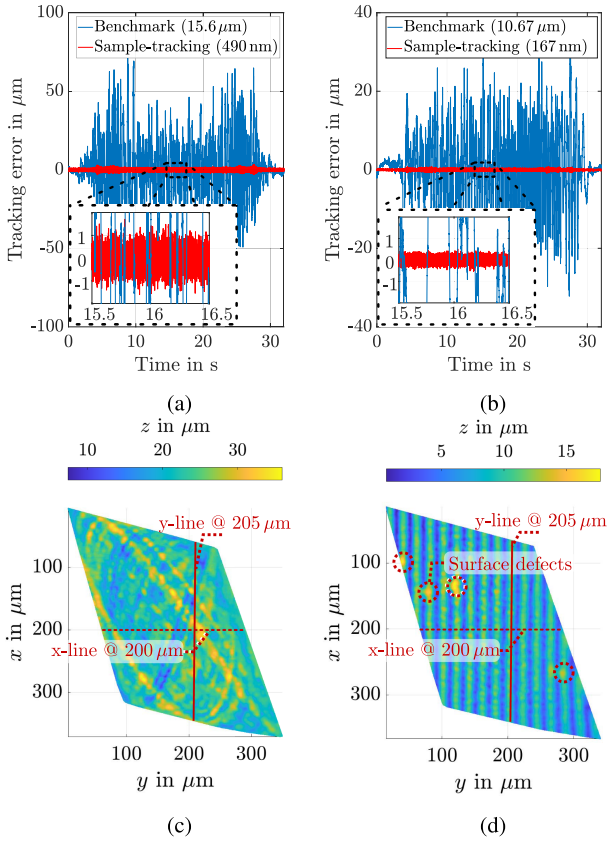

Fig. 11. Sample-tracking and 3-D measurement performance for the sample conveyed at 10 mm s^{-1}. (a) and (b) Sample-tracking performance in DOFs x and z with and without active sample-tracking control. (c) Relative motion in the benchmark scenario corrupts the 3-D measurement. (d) For active sample-tracking, the grating structure and surface defects [see Fig. 10(a)] are visible.

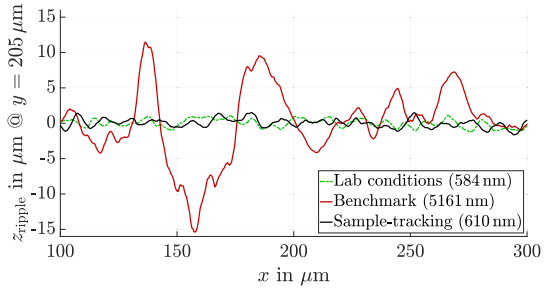

Fig. 12. Cross-sectional analysis of the 3-D measurements in Fig. 10(b) (lab conditions), 11(c) (benchmark), and 11(d) (active sample-tracking). The active sample-tracking control reduces the 3-D measurement uncertainty in motion (black) close to the uncertainty obtained in static, lab conditions (dashed green).

can be seen in Fig. 10(b), the sample height cannot be correctly reconstructed, as the spot diameter of the CCS matches the gap width of the calibration grating. As an indicator for the axial 3-D measurement performance, the height variation along the cross-section at $y = 205\ \mu$m is used.

The motion trajectory from Fig. 8 is applied to the conveyed sample. Within the interval $T_{\text{meas.}} = [t_1, t_2]$, the rms tracking errors in motion direction (DOF x) and out-of-plane (DOF z) are evaluated for the maximum sample velocity $v = 10$ mm s^{-1}. To demonstrate the effectiveness of the proposed dual stage-controlled sample-tracking system, a 3-D measurement is acquired within this time interval.

Fig. 11 shows the results of the 3-D measurements in motion, with the tracking error exemplarily shown for the sample motion direction x [see Fig. 11(a)] and the out-of-plane DOF z [see Fig. 11(b)]. In the benchmark scenario, as described at the beginning of Section V, tracking errors with rms values of 15.6 μm in DOF x and of 10.67 μm in DOF z are obtained. The relative motion between the SCCS and the sample distorts the 3-D measurement considerably [see Fig. 11(c)].

To enable high-precision 3-D measurements in motion, active sample-tracking is activated. The tracking error in Fig. 11(a) and (b) (red) is reduced to 490 nm rms in DOF x and of 167 nm rms in DOF z. This accords to a relative motion reduction by factors of 32 (motion direction x) and 64 (DOF z). The significantly reduced relative motion between SCCS and sample enables the precise 3-D surface measurement on the moving sample [see Fig. 11(d)].

By analyzing the axial measurement uncertainty (rms value) along the top of the grating structure at $y = 205\ \mu$m, the 3-D measurement performance is determined in Fig. 12. As can be seen, the high measurement uncertainty of 10μm in the benchmark scenario (red) is in the same order of magnitude as the according tracking error in Fig. 11(b). Compared to the benchmark scenario, the active sample-tracking reduces the 3-D measurement uncertainty in motion (black) by one order of magnitude to 610 nm rms and, thus, close to the uncertainty of the static, lab conditions (dashed green). To evaluate the mean pitch, the grating structure is analyzed along $x = 200\ \mu$m for all three scenarios, as exemplarily shown in Fig. 10(b). The mean pitch under static lab-like conditions is 19.97 μm, matching the pitch specified by the manufacturer. When performing 3-D measurements on a moving sample with active sample-tracking, a mean pitch of 19.46 μm is obtained, showing a mean pitch measurement error of only 500 nm. As the grating structure cannot be reasonably reconstructed in the benchmark scenario for disabled sample-tracking, the pitch evaluation cannot performed.

In summary, the dual stage-controlled positioning system reduces the long-range sample-tracking error by factor 32 down to 490 nm rms for velocities of up to 10 mm s^{-1}, enabling 3-D measurements on moving objects with submicrometer precision.

VI. Conclusion

This article presents a dual stage-controlled 6-DOF positioning system to perform high-precision 3-D measurements on samples in motion. The system comprises a sample-tracking measurement module mounted as end effector to a robotic coarse actuator. With a sample-tracking control BW of 450 Hz, the measurement module is capable of significantly reducing relative motion between the SCCS and the sample to perform 3-D images with submicrometer precision. To maintain the MP within its actuation range while tracking a moving target in six DOFs, a dual stage control architecture is designed to

reposition the robotic coarse actuator. The dynamics of the position-controlled robotic actuator are identified in different positions along the conveyor travel range. A 6-DOF robotic repositioning control with a BW of about 1 Hz is designed to enable the long-range tracking of moving samples. Experimental results at a sample velocity of 10 mm s^{-1} show that compared to the benchmark scenario, the proposed sample-tracking approach reduces the tracking error in motion direction from 15.6 μm rms to 490 nm rms. The analysis of the acquired 3-D measurement data reveals a measurement uncertainty reduction by one order of magnitude to 610 nm rms, demonstrating the system's capability to perform 3-D measurements with submicrometer precision on samples in motion. Compared to state-of-the-art robotic inline measurement systems, which typically achieve measurement accuracies in the range of tens of micrometers due to the finite positioning precision of IRs [11], [30], the proposed dual stage-controlled 6-DOF system effectively demonstrates the capability to perform inline measurements on moving objects. As a result, the achievable measurement precision is decoupled from the positioning accuracy of IRs. Future work will include extending the system's capability to perform 3-D measurements on moving free-form surfaces, as it is often required in various industries, such as the automotive sector.

REFERENCES

[1] D. Imkamp et al., "Herausforderungen und Trends in der Fertigungsmesstechnik–Industrie 4.0," *tm - Technisches Messen*, vol. 83, no. 7/8, pp. 417–429, 2016.

[2] H. Lasi, P. Fettke, H.-G. Kemper, T. Feld, and M. Hoffmann, "Industry 4.0," *Bus. Inf. Syst. Eng.*, vol. 6, no. 4, pp. 239–242, 2014.

[3] D. Imkamp, R. Schmitt, and J. Berthold, "Blick in die Zukunft der Fertigungsmesstechnik," *tm - Technisches Messen*, vol. 79, no. 10, pp. 433–439, 2012.

[4] R. Schmitt and F. Moenning, "Ensure success with inline-metrology," in *Proc. 18th IMEKO World Congr. - Metrol. Sustain. Develop.*, 2006, pp. 1–6.

[5] I. Iglesias, M. Sebastián, and J. Ares, "Overview of the state of robotic machining: Current situation and future potential," *Procedia Eng.*, vol. 132, pp. 911–917, 2015.

[6] M. Bartoš, V. Bulej, M. Bohušík, J. Stanček, V. Ivanov, and P. Macek, "An overview of robot applications in automotive industry," *Transp. Res. Procedia*, vol. 55, pp. 837–844, 2021.

[7] W. Ji and L. Wang, "Industrial robotic machining: A review," *Int. J. Adv. Manuf. Technol.*, vol. 103, pp. 1239–1255, 2019.

[8] Y. Li and P. Gu, "Free-form surface inspection techniques state of the art review," *Comput.-Aided Des.*, vol. 36, no. 13, pp. 1395–1417, 2004.

[9] S. Lemes, D. Strbac, and M. Cabaravdic, "Using industrial robots to manipulate the measured object in CMM," *Int. J. Adv. Robot. Syst.*, vol. 10, no. 7, 2013, Art. no. 281.

[10] A. Tandiya, S. Akthar, M. Moussa, and C. Tarray, "Automotive semi-specular surface defect detection system," in *Proc. 15th Conf. Comput. Robot Vis.*, 2018, pp. 285–291.

[11] E. Kiraci, P. Franciosa, G. A. Turley, A. Olifent, A. Attridge, and M. A. Williams, "Moving towards in-line metrology: Evaluation of a laser radar system for in-line dimensional inspection for automotive assembly systems," *Int. J. Adv. Manuf. Technol.*, vol. 91, no. 1–4, pp. 69–78, 2016.

[12] P. Shiakolas, K. Conrad, and T. Yih, "On the accuracy, repeatability, and degree of influence of kinematics parameters for industrial robots," *Int. J. Model. Simul.*, vol. 22, no. 4, pp. 245–254, 2002.

[13] F. Berry et al., "Light management in perovskite photovoltaic solar cells: A perspective," *Adv. Energy Mater.*, vol. 12, no. 20, 2022, Art. no. 2200505.

[14] M. Liebens et al., "In-line metrology for characterization and control of extreme wafer thinning of bonded wafers," *IEEE Trans. Semicond. Manuf.*, vol. 32, no. 1, pp. 54–61, Feb. 2019.

[15] E. Csencsics, M. Thier, S. Ito, and G. Schitter, "Supplemental peak filters for advanced disturbance rejection on a high precision endeffector for robot-based inline metrology," *IEEE/ASME Trans. Mechatron.*, vol. 27, no. 4, pp. 2258–2266, Aug. 2022.

[16] M. Thier, R. Saathof, A. Sinn, R. Hainisch, and G. Schitter, "Six degree of freedom vibration isolation platform for in-line nano-metrology," *IFAC-PapersOnLine*, vol. 49, no. 21, pp. 149–156, 2016.

[17] D. Wertjanz, E. Csencsics, T. Kern, and G. Schitter, "Bringing the lab to the fab: Robot-based inline measurement system for precise 3-D surface inspection in vibrational environments," *IEEE Trans. Ind. Electron.*, vol. 69, no. 10, pp. 10666–10673, Oct. 2022.

[18] B.-S. Kim, J. Li, and T.-C. Tsao, "Two-parameter robust repetitive control with application to a novel dual-stage actuator for noncircular machining," *IEEE/ASME Trans. Mechatron.*, vol. 9, no. 4, pp. 644–652, Dec. 2004.

[19] W. Dong, J. Tang, and Y. ElDeeb, "Design of a linear-motion dual-stage actuation system for precision control," *Smart Mater. Structures*, vol. 18, no. 9, Aug. 2009, Art. no. 095035.

[20] H. Lan, Y. Ding, H. Liu, and B. Lu, "Review of the Wafer stage for nanoimprint lithography," *Microelectronic Eng.*, vol. 84, no. 4, pp. 684–688, 2007.

[21] D. Wertjanz, T. Kern, E. Csencsics, G. Stadler, and G. Schitter, "Compact scanning confocal chromatic sensor enabling precision 3-D measurements," *Appl. Opt.*, vol. 60, no. 25, pp. 7511–7517, Sep. 2021.

[22] L. Guo, D. Martin, and D. Brunnett, "Dual-stage actuator servo control for high density disk drives," in *Proc. IEEE/ASME Int. Conf. Adv. Intell. Mechatron.*, 1999, pp. 132–137.

[23] D. Wertjanz, T. Kern, A. Pechhacker, E. Csencsics, and G. Schitter, "Robotic precision 3D measurements in vibration-prone environments enabled by active six DoF sample-tracking," in *Proc. IEEE/ASME Int. Conf. Adv. Intell. Mechatron.*, 2022, pp. 1441–1446.

[24] E. Csencsics, J. Schlarp, T. Schopf, and G. Schitter, "Compact high performance hybrid reluctance actuated fast steering mirror system," *Mechatronics*, vol. 62, 2019, Art. no. 102251.

[25] A. Karim, J. Hitzer, A. Lechler, and A. Verl, "Analysis of the dynamic behavior of a six-axis industrial robot within the entire workspace in respect of machining tasks," in *Proc. IEEE Int. Conf. Adv. Intell. Mechatron.*, 2017, pp. 670–675.

[26] J. Oaki, "Rigid-joint-model feedforward with elastic-joint-model feedback for motion control of a 6-DoF industrial robot," *IFAC-PapersOnLine*, vol. 53, no. 2, pp. 8462–8469, 2020.

[27] M. Chan, "Controller synthesis and vibration suppression techniques for industrial robotic manipulators with joint flexibilities," Ph.D. dissertation, University of California, Berkeley, Berkeley, CA, USA, 2013.

[28] S. Chander, P. Agarwal, and I. Gupta, "Auto-tuned, discrete PID controller for DC-DC converter for fast transient response," in *Proc. India Int. Conf. Power Electron.*, 2011, pp. 1–7.

[29] D. Wertjanz, E. Csencsics, and G. Schitter, "An efficient control transition scheme between stabilization and tracking task of a MAGLEV platform enabling active vibration compensation," in *Proc. IEEE/ASME Int. Conf. Adv. Intell. Mechatron.*, 2020, pp. 1943–1948.

[30] H. Kihlman, R. Loser, A. Cooke, A. Sunnanbo, and K. Von Arb, "Metrology-integrated industrial robots: Calibration, implementation and testing," in *Proc. 35th ISR Int. Symp. Robot.*, Paris, France, 2004, pp. 1–6.

Matthias Laimer received the M.Sc. degree in electrical engineering from TU Wien, Vienna, Austria, in 2022.

He is currently a Doctoral Researcher with the Automation and Control Institute (ACIN), TU Wien. His primary research interests include industrial automation and robot-based inline measurement systems.

Daniel Wertjanz received the M.Sc. degree in electrical engineering from TU Wien, Vienna, Austria, in 2019.

He is currently a Doctoral Researcher with the Automation and Control Institute, TU Wien. His primary research interests include high-performance mechatronic systems design, high-precision motion control, and robot-based inline measurement systems.

Peter Gsellmann received the M.Sc. degree in electrical engineering from TU Wien, Vienna, Austria, in 2018.

He is currently a Doctoral Researcher with the Automation and Control Institute, TU Wien. His primary research interests include industrial automation and vision-based control of industrial robots.

Georg Schitter (Senior Member, IEEE) received the M.Sc. degree in electrical engineering from TU Graz, Graz, Austria, in 2000, and the second M.Sc. degree in information technology and Ph.D. degree in technical sciences from ETH Zurich, Zurich, Switzerland, in 2004.

He is currently a Professor for Advanced Mechatronic Systems with the Automation and Control Institute (ACIN), TU Wien, Vienna, Austria. His primary research interests include high-performance mechatronic systems, particularly for applications in the high-tech industry, scientific instrumentation, and mechatronic imaging systems, such as AFM, scanning laser and LiDAR systems, telescope systems, adaptive optics, and lithography systems for semiconductor industry.

Dr. Schitter was the recipient of the journal best paper award of IEEE/ASME TRANSACTIONS ON MECHATRONICS in 2018, *IFAC Mechatronics* in 2008–2010, *Asian Journal of Control* in 2004–2005, and the 2013 IFAC Mechatronics Young Researcher Award. He was an Associate Editor for *IFAC Mechatronics*, *Control Engineering Practice*, and IEEE TRANSACTIONS ON MECHATRONICS.

Ernst Csencsics (Member, IEEE) received the M.Sc. and Ph.D. degrees (sub auspiciis) in electrical engineering from TU Wien, Vienna, Austria, in 2014 and 2017, respectively.

He is currently an Associate Professor for Measurement Systems with the Automation and Control Institute (ACIN), TU Wien. His primary research interests are on opto-mechatronic measurement and imaging systems, high performance mechatronics, scientific instrumentation, precision engineering, and advanced robotic inline measurement systems.

Dr. Csencsics was the recipient of the journal Best Paper Award of IEEE/ASME TRANSACTIONS ON MECHATRONICS (2018), the Best Paper Award at the IEEE International Instrumentation and Measurement Technology Conference (2022), and the Best Student Paper Award at the American Control Conference (2016).